BOREAS An international journal of Quaternary research

Weichselian–Holocene glacial history of the Sjuøyane archipelago, northern Svalbard

ANDERS SCHOMACKER, HELENA ALEXANDERSON, WESLEY R. FARNSWORTH, MARK F. A. FURZE, SOFIA E. KJELLMAN, NINA KIRCHNER, ELIAS STRANDELL ERSTORP, RIKO NOORMETS, VINCENT JOMELLI AND ÓLAFUR INGÓLFSSON

BOREAS

Schomacker, A., Alexanderson, H., Farnsworth, W. R., Furze, M. F. A., Kjellman, S. E., Kirchner, N., Erstorp, E. S., Noormets, R., Jomelli, V. & Ingólfsson, Ó.: Weichselian–Holocene glacial history of the Sjuøyane archipelago, northern Svalbard. *Boreas*. https://doi.org/10.1111/bor.12673. ISSN 0300-9483.

The Sjuøyane archipelago is the northernmost land area of Svalbard; thus, it provides a window to study the terrestrial glacial history and dynamics of the Svalbard–Barents Sea Ice Sheet and complement marine geological studies in the region. To reconstruct the glacial history of Sjuøyane, we describe coastal sedimentary sections in Quaternary sediments and constrain their chronology by radiocarbon and optically stimulated luminescence ages. Erratic boulders and bedrock are sampled for ^{10}Be cosmogenic exposure dating, aiming to determine the deglaciation age and exposure history. Holocene environments are studied based on lake sediments and emerging vegetation from retreating snow patches. The sedimentary sections largely consist of shallow (glacio-)marine and/or littoral sediments deposited during high relative sea levels. The radiocarbon and luminescence ages suggest they formed during a Middle Weichselian interstadial, and after the Late Weichselian glaciation. A wave-washed bedrock erosional notch and rounded boulders at 36±1 m a.h.t. most likely formed during this interstadial. Most of the cosmogenic ^{10}Be ages are older than the last deglaciation, likely indicating a complex exposure history. One boulder sample suggests that the lowlands were deglaciated 14.7±1.82 ka ago, and two boulder samples with ages of 18.94±3.26 and 22.89±4.05 ka suggest that the highlands were possibly ice-free at this time. The lake sediments from Isvatnet, Phippsøya, consist of glaciolacustrine silt and clay overlain by gyttja. The gyttja has accumulated at least since 7.0 cal. ka BP. Two radiocarbon ages from emerging vegetation suggest Neoglacial cooling since 3.8 cal. ka BP. A patchy glacial drift at the surface of Sjuøyane and well-preserved pre-Late Weichselian sediments suggest that the Late Weichselian glaciation was non-erosive and/or cold-based at this part of the north margin of the Svalbard–Barents Sea Ice Sheet.

Anders Schomacker (anders.schomacker@uit.no) and Sofia E. Kjellman, Department of Geosciences, UiT The Arctic University of Norway, Postboks 6050 Langnes, NO-9037 Tromsø, Norway; Helena Alexanderson, Department of Geology, Lund University, Sölvegatan 12, SE-223 62 Lund, Sweden; Wesley R. Farnsworth, Institute of Earth Sciences, University of Iceland, Askja, Sturlugata 7, IS-102 Reykjavík, Iceland and Globe Institute, University of Copenhagen, Øster Voldgade 5-7, DK-1350 Copenhagen K, Denmark and Nordic Volcanological Center, University of Iceland, Askja, Sturlugata 7, IS-102 Reykjavík, Iceland; Mark F. A. Furze and Riko Noormets, Department of Arctic Geology, The University Centre in Svalbard (UNIS), P.O. Box 156, NO-9171 Longyearbyen, Norway; Nina Kirchner, Department of Physical Geography, Stockholm University, SE-106 91 Stockholm, Sweden; Elias Strandell Erstorp, Department of Geological Sciences, Stockholm University, SE-106 91 Stockholm, Sweden; Vincent Jomelli, Aix Marseille University, CNRS, IRD, INRAE, CEREGE, BP 80, F-13545 Aix-en-Provence Cedex 4, France; Ólafur Ingólfsson, Institute of Earth Sciences, University of Iceland, Askja, Sturlugata 7, IS-102 Reykjavík, Iceland; *received 13th February 2024, accepted 8th July 2024.*

Marine geological data from the continental shelf north of Svalbard suggest that the Svalbard–Barents Sea Ice Sheet (SBIS) was at its Local Last Glacial Maximum (LLGM) *c*. 26 cal. ka BP, close to the continental shelf break north of Sjuøyane, northernmost Svalbard (e.g. Kleiber *et al*. 2000; Knies *et al*. 2001; Svendsen *et al*. 2004; Chauhan *et al*. 2014, 2016; Patton *et al*. 2015; Fig. 1). Mega-scale glacial lineations at the sea floor indicate LLGM ice-stream activity in the Hinlopen Trough (Ottesen *et al*. 2007; Dowdeswell *et al*. 2010; Batchelor *et al*. 2011), and subglacially elongated landforms in the Kvitøya Trough suggest that a major warm-based outlet glacier occupied this trough (Hogan *et al*. 2010). Fransner *et al*. (2017) mapped subglacially streamlined landforms in Duvefjorden and Rijpfjorden, northern Nordaustlandet, suggesting topographically controlled, rapid ice flow occurred in these fjords. The continental shelf north of Svalbard between these troughs is up to ~200 m deep (Jakobsson *et al*. 2020), and was characterized by less active, thin and possibly cold-based, glacier flow during the LLGM (Hogan *et al*. 2010). Such a LLGM configuration with fast ice flow in the troughs and less active, possibly cold-based, ice on the continental shelf is supported by numerical ice-sheet models (e.g. Patton *et al*. 2016) and conceptual glaciation models (e.g. Landvik *et al*. 1998, 2005; Ingólfsson 2011; Ingólfsson & Landvik 2013). A radiocarbon age of mixed benthic foraminifera in deglacial glaciomarine sediment, 6 cm above a diamicton in core JR142-GC13 from the upper continental slope ~65 km north of Sjuøyane provides a minimum age of 15.3 cal. ka BP for the retreat of grounded ice (Lab. no SUERC-47932; Hogan *et al*. 2017; Fig. 1, Table S1). To the east of Sjuøyane, a radiocarbon age from sediment core HH15-14 on the continental shelf suggests that the shelf west of the Albertini Trough was

DOI 10.1111/bor.12673

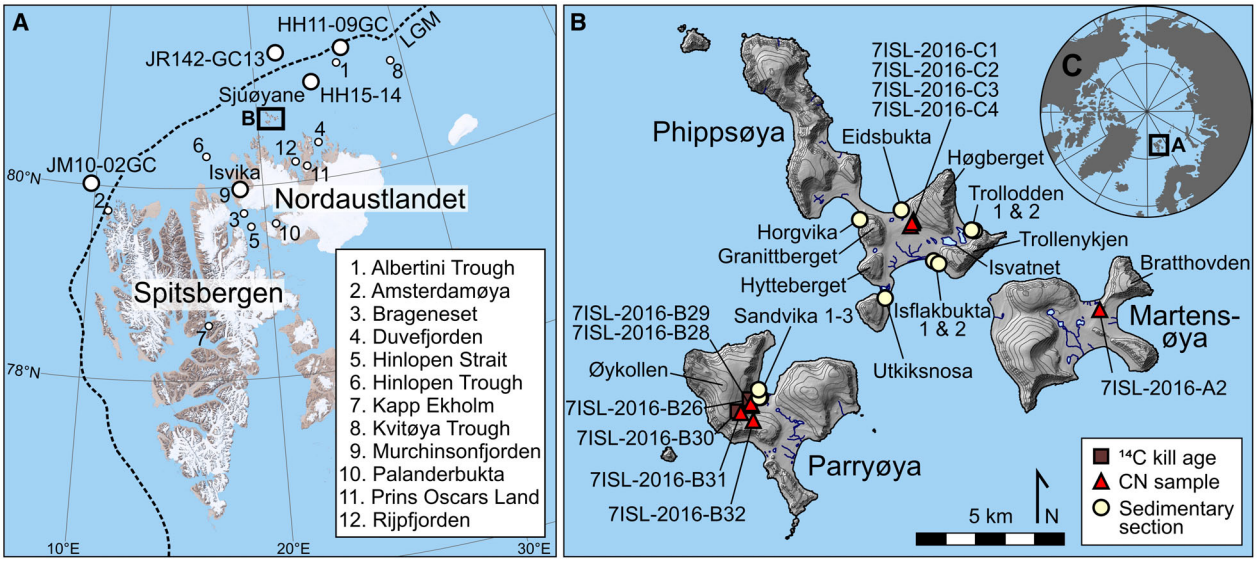

Fig. 1. A. Map of Svalbard with place names mentioned in the text. The dashed line marks the extent of the Svalbard–Barents Sea Ice Sheet during the Last Glacial Maximum (LGM) after Ingólfsson & Landvik (2013). Background map modified from Norwegian Polar Institute (2017). B. Map of the Sjuøyane archipelago with sample sites and place names mentioned in the text indicated. The terrain shaded relief model is based on a 20-m digital elevation model produced by stereophotogrammetry on aerial photographs from 2010 by the Norwegian Polar Institute (2014). The elevation contour lines are shown with 50-m intervals. C. Location of Svalbard in the Arctic.

ice-free by 15.2 cal. ka BP (Fransner *et al.* 2018; Fig. 1, Table S1).

Compared to other parts of the archipelago, few terrestrial Quaternary stratigraphical sections have been described from northeastern Svalbard. On Brageneset, Nordaustlandet, Donner & West (1957) identified tills with fabrics indicating ice flow towards the southwest into the Hinlopen Strait. Further north on Nordaustlandet, in Murchinsonfjorden, Kaakinen *et al.* (2009) described the Quaternary lithostratigraphy in Isvika (Fig. 1) and determined the ages of shallow marine sediments using radiocarbon dating and OSL dating. They identified three subglacial till beds with fabrics showing westerly ice-flow directions towards the Hinlopen Strait. This is supported by the orientation of striae on bedrock outcrops in the area. Each till bed is stratigraphically overlain by shallow marine sand and gravel. The OSL ages of the shallow marine sediments are 83.1±10.2 ka (Early Weichselian interstadial, MIS 5a), 37.0±3.7 ka (Middle Weichselian interstadial, MIS 3), and Holocene. The Middle Weichselian OSL age overlaps within the 2σ age range of 52.0–40.0 cal. ka BP (Lab. no. HELA-1653; Table S1) of radiocarbon-dated shell fragments in the same unit. The preservation of older sediments, weathered bedrock, and restricted lateral distribution of the sediments suggest that the glaciers that deposited the till beds were mainly cold-based and located east of the ice stream in the Hinlopen Strait (Kaakinen *et al.* 2009). Hormes *et al.* (2011) used cosmogenic exposure dating of 19 bedrock and erratic boulder samples in the Murchinsonfjorden area and Prins Oscars Land area on Nordaustlandet to constrain the timing of deglaciation. The ages range from 122.8±7.6 to 13.0±2.2 ka ago. The youngest dates (15.4–13.0 ka ago) provide deglaciation ages of the lowlands and fjords, and together with geomorphological evidence of subglacial erosion suggest that the glaciers were warm-based in the topographic lows. In contrast, none of the bedrock and boulder samples from the uplands and plateaux yielded ages from the last deglaciation. Seven of these have MIS 3 ages, and the remaining are older. These ages probably indicate a complex exposure history and inherited isotopes in the samples. Based on these ages and glacial geological mapping, Hormes *et al.* (2011) concluded that the higher elevation parts (>~200 m a.s.l.) of Nordaustlandet were covered by cold-based ice in MIS 2, and that uplands in Prins Oscars Land might not have been glaciated since MIS 4. The large-scale spatial pattern of postglacial glacio-isostatic rebound reconstructed from raised beaches on Svalbard shows a decreasing ice load towards the north on Nordaustlandet and Sjuøyane (e.g. Blake 1961; Bondevik 1993; Forman & Ingólfsson 2000; Forman *et al.* 2004; Schomacker *et al.* 2019). Forman *et al.* (2004) proposed a 2–6 ka duration of LLGM glacier ice cover along the north margin of the SBIS, north of Sjuøyane.

The Sjuøyane archipelago, north of Nordaustlandet is the northernmost land area of Svalbard, and a key – yet understudied – site to reconstruct the glacial history and dynamics of the northern margin of the Weichselian SBIS. This paper aims to reconstruct the Weichselian and Holocene glaciation history of Sjuøyane using lithostratigraphy and geochronology of sedimentary sections

and lake sediments as well as cosmogenic exposure dating of bedrock and boulders to constrain the timing of the deglaciation. Further, we discuss our results in the context of previous marine and terrestrial studies in the area. Our terrestrial data provide new insight into the geomorphology, lithology, lateral distribution, and chronology of the Quaternary deposits on Sjuøyane. Thus, they complement earlier marine sediment studies, which mainly focus on the timing of deglaciation and palaeoceanography of the region.

Background

Setting

Sjuøyane is an archipelago (latitude ~80.7°N, longitude 20.9°E) north of Nordaustlandet, northeastern Svalbard (Fig. 1). A ~30-km-wide strait separates Sjuøyane from Nordaustlandet, and the continental shelf between Sjuøyane and Nordaustlandet is ~50–100 m deep (Jakobsson *et al*. 2020). To the north, the archipelago is exposed towards the Arctic Ocean. The bedrock is mainly migmatites of the Mesoproterozoic Duvefjorden Complex and Caledonian granites of the Rijpfjorden Granitoid Suite (Dallmann 2015). The islands are glacially sculpted and consist of individual mountain summits up to 464 m a.s.l. The summits on each island are connected by lowlands of raised beach ridge plains, glacial drift, talus, and locally weathered bedrock (Fig. 2). The largest lake in the archipelago, Isvatnet, is located 33 m a.s.l. in the lowlands between mountains Høgberget and Trollenykjen, Phippsøya (Figs 1B, 2B).

Glaciation history

Forman & Ingólfsson (2000) described gentle south-facing mountain slopes and steep north-facing slopes on Phippsøya, indicating glacial overriding from a southerly direction during Quaternary glaciations. This interpretation is supported by erratic boulders of granite with a provenance from Nordaustlandet occurring on Sjuøyane (Salvigsen & Nydal 1981; Forman & Ingólfsson 2000). A patchy glacial drift occurs on Sjuøyane above the postglacial marine limit. It contains marine shell fragments suggesting that glaciers eroded the surrounding shelf before depositing the drift. Two median radiocarbon ages of 42.7 (Lab. no. GX-22385-AMS) and 42.0 cal. ka BP (Lab. no. T-3102) from shell fragments in the drift provide its maximum age (Salvigsen & Nydal 1981; Forman & Ingólfsson 2000; Table S1). Few stratigraphical sections are available along the coasts of the islands, e.g. at the southern part of Phippsøya. Forman & Ingólfsson (2000) described a 4-m-high section on Phippsøya, and identified shallow marine sands deposited during high relative sea level. A radiocarbon age of a *Hiatella arctica* shell in the sands yields a median age of 50.5 cal. ka BP (Lab. no. GX-22388; Forman & Ingólfsson 2000; Table S1). The postglacial marine limit on Phippsøya is located at 22±1 m above high tide (a.h.t.) and raised beaches indicate glacio-isostatic rebound following the Late Weichselian glaciation (Salvigsen & Nydal 1981; Forman & Ingólfsson 2000). The age of the postglacial marine limit is not well defined but is constrained by a minimum age of 10.6 cal. ka BP of a *Balanus balanus* at 10 m a.h.t. (Lab. no. GG-22386; Forman & Ingólfsson 2000; Table S1). There are currently no glaciers on Sjuøyane, but perennial snow patches persist, and in some cases are located just above sea level. Leirdal (1997) estimated an ice-marginal position 15–20 km north of Sjuøyane during the Late Weichselian.

Material and methods

Bathymetry and lake sediment coring

The bathymetry of Isvatnet, Phippsøya (80.70°N, 20.96°E, 33 m a.s.l.; Fig. 1B) was surveyed in August 2018 with an autonomous surface vehicle (ASV) developed as part of a fleet of maritime robots at the Department of Naval Architecture at KTH Royal Institute of Technology, Stockholm. The ASV's standard payload comprises a GPS receiver, motion sensor, and an EchoRange Smart SS510 single beam echo-sounder for bathymetric mapping of shallow waters, which it carries out on a predefined, mission-specific horizontal grid with a user-defined and application-specific mesh cell size. Given the ASV's typical speed of 1.75 kn (~0.9 m s^{-1}), and the 1-Hz transmit frequency of the echo-sounder, the resolution of the bathymetric data acquired here is on the order of 1 sounding per metre along path, and 1 sounding per 10–20 m across path. The acquired georeferenced soundings are transformed from time to depth using a sound velocity of 1426 m s^{-1} for freshwater at 5 °C. For further details, see Kirchner *et al.* (2019) and Vacek *et al.* (in press).

Two short sediment cores were retrieved from the deepest part of the lake basin. The coring was performed through a hole in the floor of a zodiac, which was anchored at a stable position. A Universal percussion sediment corer from Aquatic Research Instruments was used to obtain a 38-cm-long core (IVS2) and a 34-cm-long core (IVS3), both with 68-mm diameter.

Sedimentological analyses

Lake sediment cores were split open, lithostratigraphically logged, and photographed with a RGB line scan camera mounted on an Aavatech core scanner. X-ray imagery was recorded using a Geotek Standard X-ray CT System (XCT). Samples for radiocarbon dating were collected from core IVS3.

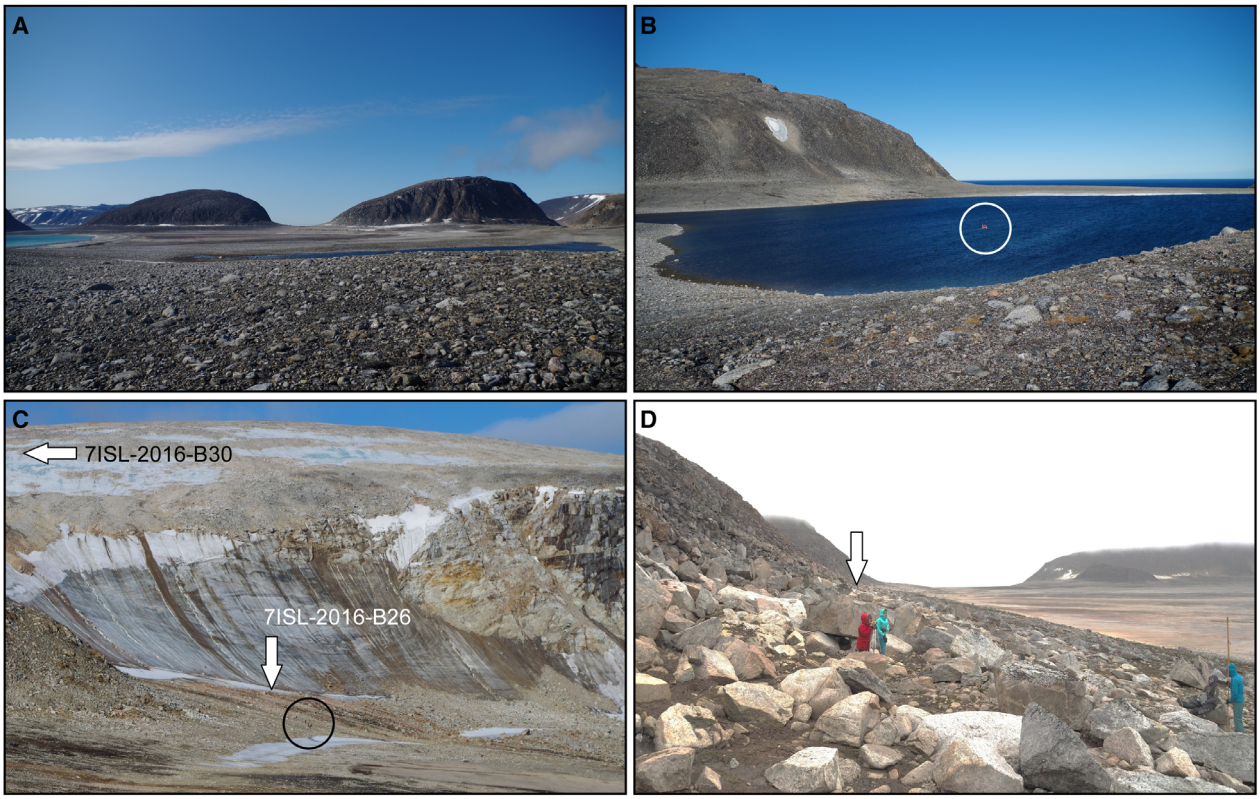

Fig. 2. Geomorphology of Sjuøyane. A. View towards the southwest across Isflakbukta. Hytteberget and Granittberget are seen in the background. 2nd August 2016. B. Isvatnet seen towards the north. Note the zodiac (circled) on the lake for scale. 2nd August 2016. C. View towards the west of the perennial snow patch at Øykollen, Parryøya. Sample positions are marked with arrows. The circle shows persons for scale. 4th August 2016. D. Erosional bedrock notch (arrow) at the foot of Hytteberget in Isflakbukta, Phippsøya, 21st August 2018. The bedrock notch is oriented in the view direction of the photograph, and the two persons are standing on it.

Coastal sedimentary sections were excavated and described in the field by logging, documentation of lithofacies, sediment texture and structure, directional elements, and fossils (e.g. Eyles *et al.* 1983; Evans & Benn 2004). Samples for OSL dating and radiocarbon dating were collected from these sections.

Radiocarbon dating

To establish the chronology of the lake sediment cores and geological sections, plant macrofossils and marine bivalve shells were collected. Additionally, two samples of *in situ* moss emerging at the margin of a ~200-m-long, perennial snow patch in the mountain slope in southwest Sandvika, Parryøya (Fig. 1B), were collected. These samples were collected at 260 and 57 m a.s.l., respectively. Plant macrofossil samples from lake sediment core IVS3 were taken from the residues of 0.25-mm sieving, isolated, and described using a binocular microscope. All samples were accelerator mass spectrometry (AMS) radiocarbon dated at the Ångström Laboratory, Uppsala University. The ages were calibrated in OxCal v4.4. using the IntCal20 and Marine20 calibration curves for terrestrial and marine samples, respectively (Heaton *et al.* 2020; Reimer *et al.* 2020). For marine ages, we applied a ΔR value of -61 ± 37 years, calculated for shells from western Svalbard (Pieńkowski *et al.* 2022). The relationship between depth and age of the lake sediment cores was established with the Bayesian-based code 'Bacon' (v.2.5.7; Blaauw & Christen 2011) in R (v.4.1.3; R Core Team 2021). All reported ages are in calibrated years before present ('cal. a BP'; BP = AD 1950).

Luminescence dating

Nineteen samples for luminescence dating were taken in opaque tubes that were hammered horizontally into exposed sediment faces, specifically sandy beds, on Phippsøya and Parryøya (Fig. 1). The samples were opened and analysed in the Lund Luminescence Laboratory, Lund University, Sweden. Details of the analytical procedure are presented in Data S1 and Figs S1–S4, and only a short description is given here. The equivalent dose (D_e) was determined from 2-mm aliquots of 180–250 μm K-feldspar grains by applying a post-IR_{50} $IRSL_{225}$ (pIRIR) single aliquot regeneration (SAR) protocol according to Buylaert *et al.* (2009) in Risø TL/OSL readers model DA-20. For one sample

(16029), 1-mm aliquots were also used. The suitability of the protocol for these samples was tested in dose recovery experiments, and fading rates and residual doses were also determined (Data S1). Between 8 and 36 aliquots were measured for D_e for each sample and they were accepted if they had a recycling ratio within 10% of unity, a test dose error <10% and recuperation <5% of the natural signal. The mean D_e of the accepted aliquots for each sample was used for age calculation.

Sediment dose rates were determined by gamma spectrometry at the Nordic Laboratory for Luminescence Dating/DTU Risø, Denmark. An internal K-content of 12.5% was assumed (Huntley & Baril 1997). Subsamples were weighed in their natural state, when saturated and when dry to determine field and saturated water content. The average water content since time of deposition is assumed to be close to saturation (based on at least partly permafrozen coastal setting or covered by ice sheet). The total environmental dose rate (Table S2) and the age for each sample were calculated in the online DRAC v.1.2 calculator (Durcan *et al.* 2015). Fading-corrected ages were calculated according to Huntley & Lamothe (2001) and using the function calc_FadingCorr in the R Luminescence package (Kreutzer 2018).

Cosmogenic nuclide dating

Nine samples were collected from Martensøya, Parryøya, and Phippsøya (Fig. 1B). We sampled bedrock and boulders on high terrain surfaces or small bedrock knobs. All samples are above the marine limit. To minimize the risk of inherited isotopes from previous exposures, we targeted erratic boulders, assuming that they had not been previously exposed to cosmic radiation (Briner *et al.* 2006; Corbett *et al.* 2013). However, suitable boulders (i.e. large, stably lodged, not weathered) are very few, and we therefore also sampled bedrock. If glacial erosion of the bedrock surface was insufficient to remove inherited isotopes, this might result in overestimated exposure ages (e.g. Gjermundsen *et al.* 2015). It is unlikely that any snow, sediment or vegetation has covered the sample sites, since they are located at small summits where wind prevents snow accumulation during winters. There is no field evidence of a sediment cover at or near the sampling sites. The topographic shielding was measured in the field with a compass and clinometer, and correction values calculated according to Balco *et al.* (2008).

Samples were crushed and sieved at UiT The Arctic University of Norway, and subsequently processed for ^{10}Be extraction at LN2C (CEREGE, France) following chemical procedures adapted from Merchel & Herpers (1999). The ^{10}Be/^{9}Be ratio measurements were performed at the ASTER AMS national facility (CEREGE, Aix-en-Provence). Samples were calibrated against the in-house standard STD-11 (^{10}Be/^{9}Be = 1.191±0.013 × 10^{-11}; Braucher *et al.* 2015) and a ^{10}Be half-life of 1.387±0.0012 × 10^{6} years (Chmeleff *et al.* 2010; Korschinek *et al.* 2010). All ^{10}Be/^{9}Be isotope ratios are reported following the 07KNSTD standardization (Nishiizumi *et al.* 2007), and ^{10}Be ages were calculated using the CREp online calculator (Martin *et al.* 2017) with a time-invariant scaling scheme for spallation (Lal 1991; Stone 2000), assuming no denudation and the Arctic production rate of 3.96±0.15 atoms g^{-1} $year^{-1}$ (Young *et al.* 2013). We decided to use the Lal/Stone scaling scheme for spallation since the influence of the Earth's magnetic field on the ^{10}Be production rate is negligible at the high latitude of Sjuøyane (~80°N; Gosse & Phillips 2001). The Arctic production rate (Young *et al.* 2013) was applied because it is generated from and tested against independent chronologies in comparable settings to Sjuøyane (i.e. high northern latitudes and low altitudes). We report individual ages with their associated uncertainties that include the standard deviations of both analytical ('internal') and production rate ('external') uncertainties when comparing to other studies or ages.

Results and interpretation

The lake sedimentary record, Isvatnet, Phippsøya

The bathymetric survey of Isvatnet showed that the lake has two bowl-shaped sub-basins (Fig. 3C). The southeastern basin reaches a water depth of ~6.5 m, and the northwestern basin reaches ~12 m water depth. Sediment cores IVS2 (38 cm long) and IVS3 (34 cm long) were obtained from the floor of the deeper, northwestern basin at a water depth of ~11 m.

We identified two main sedimentary facies in the sediment cores: dark to light grey silty clay and clayey silt, and olive-brown laminated gyttja (Fig. 3A). We focus on core IVS3, which is the core we radiocarbon dated (Table 1, Fig. 3). The lowermost lithological unit (LU 1) can be subdivided into LU 1a (34–21 cm) and LU 1b (21–15 cm). LU 1a consists of structureless massive dark grey to grey silty clay with an outsized clast in the bottom preventing us from penetrating further. LU 1b consists of light grey clayey silt and appears structureless to the naked eye, but the X-ray reveals tilted layers. LU 1 is lacking age constraints due to the absence of dateable material, but interpreted to represent glaciolacustrine sedimentation. The contact between LU 1 and the overlying unit LU 2 (15–0 cm) is sharp. We interpret this to reflect a hiatus due to a period of nondeposition and/or erosion of underlying sediments. The contact was sharp in both IVS2 and IVS3. The uppermost 15 cm of IVS3 consists of 2–6 mm thick laminae of gyttja with high content of aquatic bryophytes. The lowermost ^{14}C date in LU 2 (14–15 cm; Lab. no. Ua-71538) has a calibrated median age of 7.0 cal. ka BP (Table 1), and the age-depth model suggests continuous organic accumulation

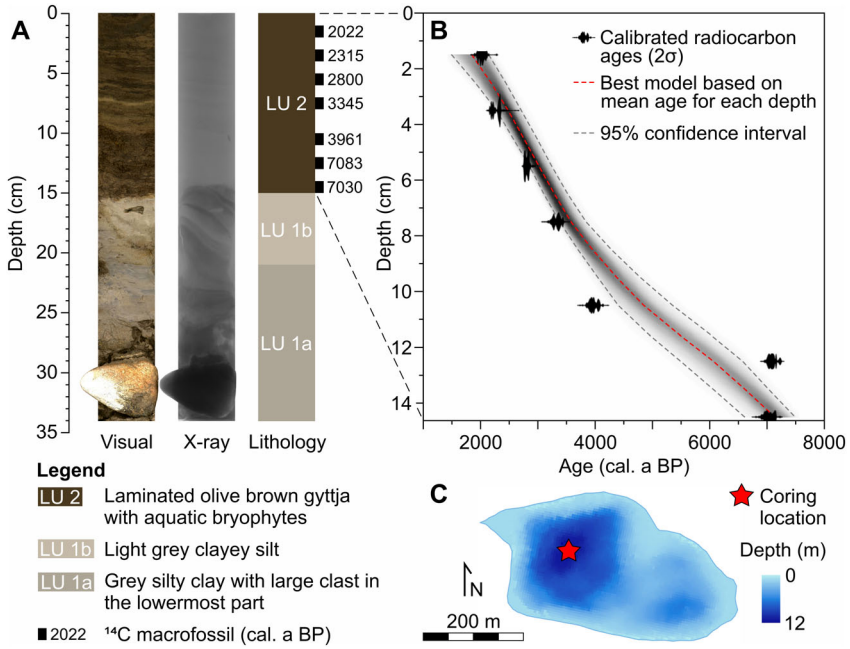

Fig. 3. A. Core photograph, X-ray image, sedimentological log, and calibrated radiocarbon ages for lake sediment core IVS3 from Isvatnet, Phippsøya. B. Age-depth model for the upper part of the core (lithological unit 2). Details on the radiocarbon ages are given in Table 1. C. Bathymetry of Isvatnet, with the coring location indicated.

through the rest of the Holocene (Fig. 3B). There is no sedimentological evidence of Neoglacial cooling.

Radiocarbon ages of moss emerging from snow patch in Sandvika, Parryøya

Sample 7ISL-2016-B30 (Lab. no. Ua-54605; 260 m a.s.l.) has a median age of 3.8 cal. ka BP and sample 7ISL-2016-B26 (Lab. no. Ua-54604; 57 m a.s.l.) has a median age of 2.8 cal. ka BP (Table 1). We interpret these ages as indicating that the snow patch was expanding at this time, thereby killing the moss growing at the surface (Fig. 2C).

Lithostratigraphy of coastal sections

Five sedimentary sections were studied on Phippsøya and three on Parryøya. On Phippsøya, coastal sections were investigated in Isflakbukta, Trollodden, Horgvika, Utkiksnosa, and Eidsbukta (Fig. 1B). In Sandvika, Parryøya, small streams fed by snow meltwater have eroded sections into landforms with a near-horizontal surface. They occur below the marine limit, ~200 m from the present coastline (Fig. 1B). We identified four lithofacies associations (LA) in the sections based on their appearance in the field (architecture, boundaries, texture, structures, and fossil content; Figs 4, 5).

LA 1 is a massive, matrix-supported silty-sandy diamict. It is observed at the base of the sections Isflakbukta 1 and Horgvika, where it transitions into permafrost. Therefore, no basal contacts are visible. In Isflakbukta, the matrix of the diamict shows normal grading. At Horgvika, paired shells, whole shells, and shell fragments of bivalves occur in the diamict. The clasts are of varied lithology. Further, LA 1 consists of a bi-modal sediment of boulders and massive sand with shell fragments observed at Horgvika. The Horgvika site (Fig. 4A) was also described by Salvigsen & Nydal (1981) and Forman & Ingólfsson (2000).

LA 1 has not been sufficiently investigated to allow a detailed genetic interpretation of the diamict (e.g. Eyles *et al.* 1983; Krüger & Kjær 1999; Benn & Evans 2010). The diamict might be deposited in a glacial or glaciomarine environment, and the bivalve shells and shell fragments suggest that the sediment originates from shallow marine or littoral deposits. The boulders in the bi-modal sediment in the upper part of LA 1 at Horgvika could have originated as rockfall material from the slopes above the sections entering a shallow marine or littoral setting (in agreement with Forman & Ingólfsson 2000).

LA 2 consists of beds of sand, gravelly sand, and silty sand (Figs 4, 5). Occasional beds of slightly coarser (i.e. gravel) and finer (i.e. silt) sediment occur. In Eidsbukta the upper part of LA 2 consists of beds of sandy-gravelly bi-modal sediment. Each bed is 5–65 cm thick. Most of the sand and gravelly sand beds are massive, although ripple-laminated sand and laminated sand are present in the Isflakbukta 2 and Trollodden 2 sections. Paired shells, whole shells, and shell fragments of bivalves (mainly *Mya truncata*) are observed frequently in LA 2. The LA has a lateral extent of 200–300 m at Isflakbukta and Trollodden. LA 2 also appears in three sections (Sandvika 1–3) in

Table 1. Radiocarbon ages from Sjuøyane, Svalbard, calibrated in OxCal v4.4. with IntCal20 (Reimer *et al.* 2020) or Marine20 (Heaton *et al.* 2020) and a ΔR value of −61±37 years for shells (Pieńkowski *et al.* 2022).

Sample	Location	Latitude and longitude (decimal degree)	Material dated	Lab. ID	Elevation (m a.s.l.) or *Core depth (midpoint; cm)*	^{14}C age (a BP)	Calibrated median age (cal. a BP)	Calibrated 2σ age ranges (cal. a BP)	δ^{13}C (‰ VPDB)
Phippsøya									
7ISL-2016-A-06	Utkiksnosa	80.6844°N, 20.8623°E	Paired bivalve shell	Ua-54598	7	>40 000	–	–	+2.1
7ISL-2016-D-1	Isflakbukta 1	80.6953°N, 20.9368°E	Shell in living position	Ua-54600	3.2	9621±41	10 412	10 626–10 216	+1.5
IVS3_1_2	Isvatnet	80.7000°N, 20.9600°E	Aquatic bryophytes	Ua-71532	*1.5*	2063±29	2022	2112–1939	−30.1
IVS3_3_4	Isvatnet	80.7000°N, 20.9600°E	Aquatic bryophytes	Ua-71533	*3.5*	2292±34	2315	2355–2300, 2251–2157	N/A
IVS3_5_6	Isvatnet	80.7000°N, 20.9600°E	Aquatic bryophytes	Ua-71534	*5.5*	2699±30	2800	2854–2755	−23.0
IVS3_7_8	Isvatnet	80.7000°N, 20.9600°E	Aquatic bryophytes	Ua-71535	*7.5*	3126±43	3345	3447–3231	N/A
IVS3_10_11	Isvatnet	80.7000°N, 20.9600°E	Aquatic bryophytes	Ua-71536	*10.5*	3644±37	3961	4086–3871, 3859–3850	N/A
IVS3_12_13	Isvatnet	80.7000°N, 20.9600°E	Aquatic bryophytes	Ua-71537	*12.5*	6201±33	7083	7245–7210, 7170–6992	−20.4
IVS3_14_15	Isvatnet	80.7000°N, 20.9600°E	Aquatic bryophytes	Ua-71538	*14.5*	6136±42	7030	7160–6901	N/A
Parryøya									
7ISL-2016-C-9	Sandvika 2	80.6485°N, 20.6400°E	Paired *Mya truncata*	Ua-54599	7	9819±43	10 700	11 001–10 482	+2.9
7ISL-2016-B-26	Sandvika	80.6479°N, 20.6211°E	Moss	Ua-54604	57	2649±33	2761	2848–2814, 2791–2728	−25.9
7ISL-2016-B-30	Sandvika	80.6442°N, 20.6038°E	Moss	Ua-54605	260	3551±33	3844	3965–3947, 3927–3816, 3800–3719	−23.6

Sandvika, Parryøya (Figs 1B, 5), and consists of massive or planar-bedded gravel and sand. The Sandvika 1 section comprises a 2-m-thick coarsening-upward succession of mainly planar beds, each 10–40 cm thick and dipping towards the north. Sandvika 2 contains paired *Mya truncata* shells.

We interpret LA 2 as deposited in shallow (glacio-) marine or littoral environments. The gravel, gravelly sand, and sand beds are deposited in beach-face and/or shore-face environments, and the fines and ripple-laminated and laminated sand beds in a shallow marine environment (Mangerud *et al.* 1998; Alexanderson *et al.* 2011). The ripple-laminated sand indicates deposition in shallow marine conditions affected by waves and/or strong bottom currents (e.g. Ó Cofaigh & Dowdeswell 2001). In Sandvika, LA 2 possibly represents foreset beds in a delta prograding towards the north, and deposited during regression (e.g. Mangerud *et al.* 1998; Alexanderson *et al.* 2011).

LA 3 is a massive, matrix-supported sandy-gravelly diamict. It occurs in the Utkiksnosa and Isflakbukta 1 sections where it is 1–2 m thick. Large clasts appear subrounded and are of local lithology. One clast with attached barnacle fragments (*Balanus* sp.) was observed.

The massive appearance and the subrounded clasts suggest that LA 3 is deposited in a glacial environment, although the diamict has not been sufficiently investigated to allow a detailed genetic interpretation (e.g. Eyles *et al.* 1983; Krüger & Kjær 1999; Benn & Evans 2010). The barnacle fragments suggest that the clasts are reworked from shallow marine or littoral deposits.

LA 4 consists of gravelly sand, gravel, cobbles, and boulders and is 25 cm to more than 160 cm thick (Fig. 4). The beds are massive, and there is a coarsening-upwards trend in grain size. At Isflakbukta 2 and Trollodden 2, normal graded, cross-planar beds of rounded cobbles and boulders dip gently offshore from each site (towards the northwest and northeast, respectively; Fig. 4D, E). The lithofacies association can be followed laterally for ~300 m in Isflakbukta and Trollodden and has an erosive or conformal basal contact.

We interpret LA 4 as prograding beach-face sediments deposited during regression. The relatively poor sorting suggests a large sediment input and/or rapid sedimentation (Bluck 1999; Strzelecki *et al.* 2018). The northwest-dipping beds in Isflakbukta and the northeast-dipping beds at Trollodden indicate that the sediments were

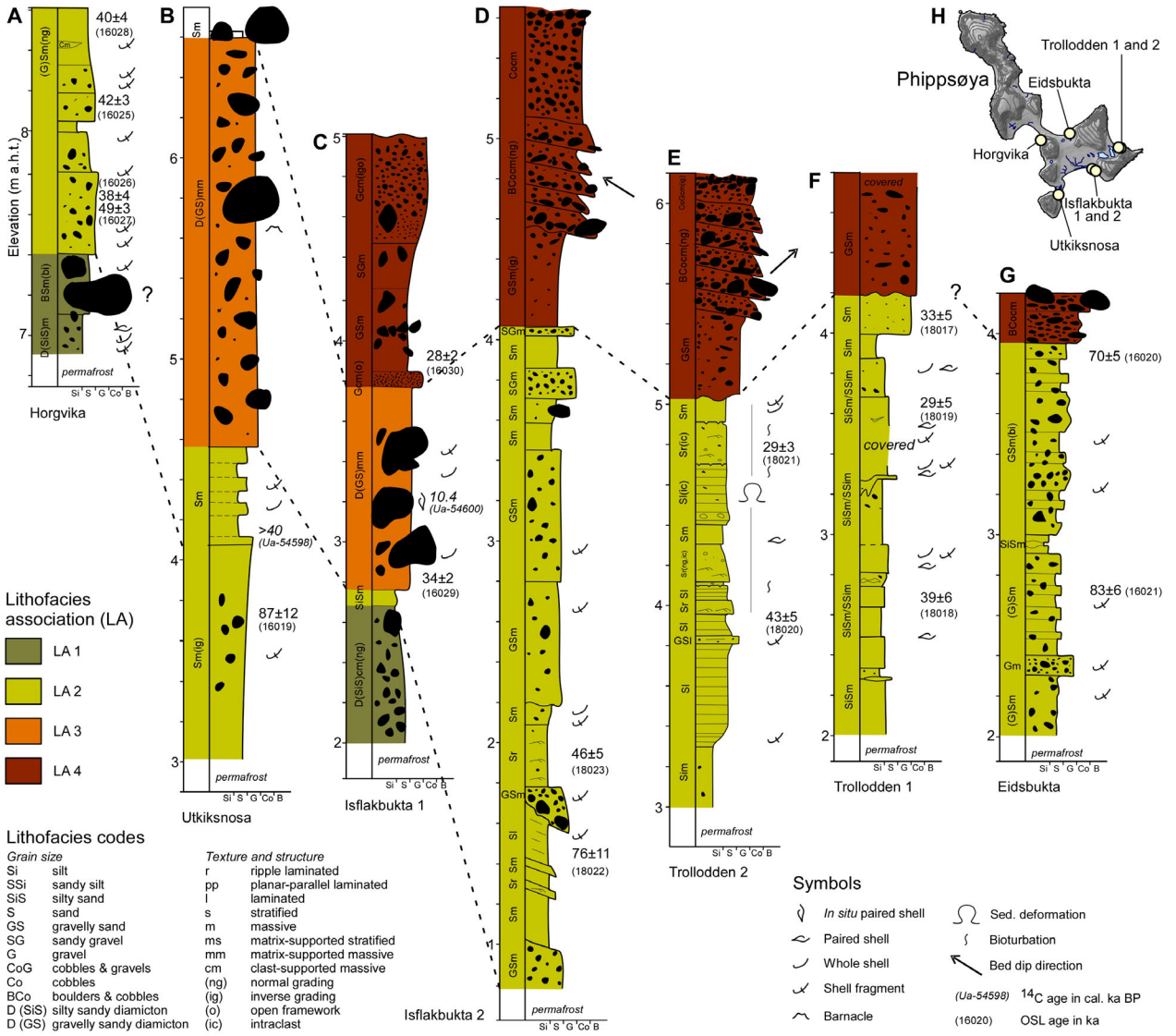

Fig. 4. A–G. Sedimentological logs from the sections on Phippsøya. The locations of the sections are shown in Fig. 1B. Details on radiocarbon ages (italics) and OSL ages are provided in Tables 1, 2. H. Overview map of Phippsøya with the locations of the sections.

building into the bays during deposition (e.g. Mangerud *et al.* 1998; Alexanderson *et al.* 2011).

The sections in Sandvika, Isflakbukta, Trollodden, and Eidsbukta reveal clear shallowing-upward successions of (glacio-)marine deposits (Figs 4, 5), which we interpret as indicating sedimentation during regression caused by glacio-isostatic rebound (e.g. Mangerud *et al.* 1998; Alexanderson *et al.* 2011). The sections at Utkiksnosa and Isflakbukta 2 possibly reflect two such successions.

Radiocarbon and luminescence ages from the sedimentary sections

Two radiocarbon ages were obtained from the sections on Phippsøya, yielding an age of >40 cal. ka BP for LA 2 (Fig. 4B, Table 1; Lab. no. Ua-54598), and a median age of 10.4 cal. ka BP for LA 3 (Fig. 4B, Table 1; Lab no. Ua-54600), respectively. Additionally, one radiocarbon age was obtained from LA 2 on Parryøya, yielding a median age of 10.7 cal. ka BP (Fig. 5B, Table 1; Lab. no. Ua-54599).

We prefer using the pIRIR ages, since they are generally considered more stable than IR_{50} ages, which fade and, hence, underestimate the age (Buylaert *et al.* 2009; Table 2, Figs 4, 5). However, the pIRIR signal bleaches more slowly than the IR_{50} (and OSL) signal and therefore runs a greater risk of suffering from incomplete bleaching and age overestimation in depositional environments where this may be a problem (Alexanderson & Murray 2012; Kars *et al.* 2014). Analysis of modern sediments from Sjuøyane show close

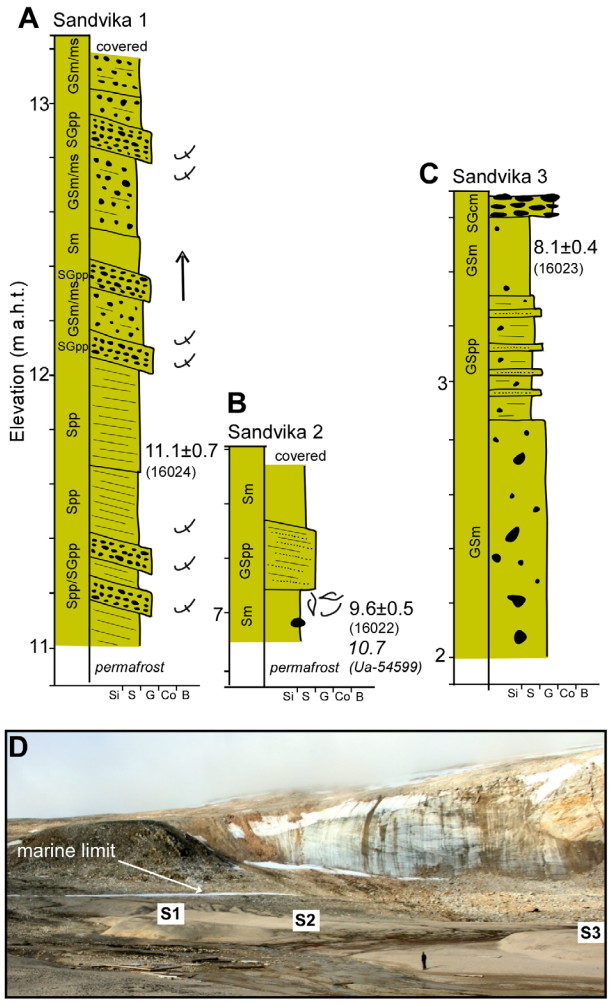

Fig. 5. A–C. Sedimentological logs from the sections in Sandvika, Parryøya. The locations of the sections are shown in Fig. 1B. D. View towards the southwest of the study site. Person for scale. For lithofacies codes and legend to symbols, see Fig. 4. Details on radiocarbon ages (italics) and OSL ages are provided in Tables 1, 2.

to zero year $pIRIR_{225}$ ages (H. Alexanderson, unpublished), which supports sufficient bleaching, while, in contrast, residual doses ('unbleachable component') are high for some samples (up to 88 Gy; Table S3). Dose recovery results also show that $pIRIR_{225}$, at least for some samples, may overestimate the true dose, while the IR_{50} may underestimate high doses (Data S1). Given these uncertainties, both IR_{50} and $pIRIR_{225}$ ages need to be treated with some caution.

We obtained 14 luminescence ages from the shallow (glacio-)marine or littoral sediments constituting LA 2 on Phippsøya (Fig. 4, Table 2), and three luminescence ages from LA 2 in the Sandvika sections, Parryøya (Fig. 5, Table 2). The luminescence ages range from 87±12 ka at the base of the Utkiksnosa section to 29±3 ka at the upper part of the LA 2 sediments at Trollodden 2. Ten of the 14 samples yield ages within MIS 3, and we interpret the sediments to be deposited during

Table 2. Luminescence ages from Sjuøyane. See also Data S1.

Site	Lab. ID	IR50 age (ka)	No. of aliquots	pIRIR225 age (ka)	No. of aliquots
Utkiksnosa	16019	105.6±9.4	8/9	87±12	8/9
Eidsbukta	16020	71.4±5.6	12/13	69.6±5.4	10/13
Eidsbukta	16021	68.0±4.8	11/12	82.8±6.1	10/12
Sandvika 2	16022	8.4±0.5	11/11	9.6±0.5	10/11
Sandvika 3	16023	6.1±0.3	14/14	8.1±0.4	14/14
Sandvika 1	16024	9.1±0.4	12/12	11.1±0.7	12/12
Horgvika	16025	38.6±2.3	12/12	42.3±3.4	10/12
Horgvika	16026	38.3±3.5	12/12	37.5±3.7	10/12
Horgvika	16027	49.3±2.8	12/12	48.7±3.4	10/12
Horgvika	16028	36.7±3.3	11/12	40.2±3.6	11/12
Isflakbukta 1	16029	22.4±1.9	15/15	33.6±2.3	10/15
Isflakbukta 1	16030	18.9±1.3	11/11	28.1±2.1	10/11
Trollodden 1	18017	37.6±3.7	15/15	32.8±5.2	15/15
Trollodden 1	18018	45.9±2.6	15/15	39.1±6.0	15/15
Trollodden 1	18019	33.8±2.0	15/15	28.9±5.4	12/15
Trollodden 2	18020	41.8±2.6	19/19	42.5±5.2	17/19
Trollodden 2	18021	28.0±1.7	15/15	29.3±3.2	15/15
Isflakbukta 2	18022	139±17	18/18	76±11	15/18
Isflakbukta 2	18023	109.7±7.4	12/12	46.3±5.1	10/12

MIS 3. The remaining four ages range from 87 to 70 ka, and are regarded as overestimated, likely because of incomplete bleaching (e.g. Alexanderson & Murray 2012). The non-finite radiocarbon age (>40 ka BP; Lab. no. Ua-54598) from LA 2 at Utkiksnosa overall agrees with the MIS 3 luminescence ages (Fig. 4, Tables 1, 2). The ages from Sandvika are 11.1±0.7, 9.6±0.5 and 8.1±0.4 ka. They agree well with the median age of 10.7 cal. ka BP of radiocarbon age Ua-54599 (Table 1), which supports the accuracy of the $pIRIR_{225}$ ages. We therefore interpret the LA 2 sediments in Sandvika as deposited during the Early Holocene.

Only one sample from the base of LA 3 was collected for luminescence dating from the Isflakbukta 1 section (Fig. 4C, Table 2). It yields a mean age of 34±2 ka. Radiocarbon age Ua-54600, collected from LA 3 in the same section (Fig. 4C, Table 1) gives a median age of 10.4 cal. ka BP. This radiocarbon age does not agree with the $pIRIR_{225}$ age of 34±2 ka (sample 16029); neither does it agree with a $pIRIR_{225}$ age of 28±2 ka (sample 16030) from the base of LA 4 in the same section (Fig. 4C, Table 2). Minimum age modelling of small (1-mm) aliquot data from sample 16029 is not able to extract an age consistent with the radiocarbon age (Table 2). Additionally, the agreement of the uncorrected $pIRIR_{225}$ age (34±2 ka; Table 2) and the fading corrected IR_{50} age (32±3 ka; Table S4) for this sample lends support to its accuracy. Because of the stratigraphical context of the radiocarbon sample, we regard it as too young although the technical quality of the sample is normal. This is because the LA 3 sediments are overlain by prograding beach-face sediments (LA 4) deposited during regression, i.e. a typical deglacial sediment (Mangerud *et al.* 1998; Alexanderson *et al.* 2011). Further, LA 4 at Isflakbukta 1 correlates with similar facies associations to the north and east (Fig. 4C, G).

Geomorphological evidence of a high relative sea level

The foot of Hytteberget in western Isflakbukta, Phippsøya (Fig. 1B) is characterized by a clear bedrock erosional notch with wave-eroded bedrock, large water-worn boulders, and rounded cobbles (Fig. 2D). In many places, the rounded boulders and cobbles are partially overlain by angular clasts from the cliff above due to frost shattering and rockfalls. The elevation of this erosional notch was surveyed to 36±1 m a.h.t. This elevation is higher than the established postglacial marine limit at 22±1 m a.h.t. (Forman & Ingólfsson 2000). We interpret the erosional notch as formed prior to the postglacial marine limit; most likely during a Weichselian interstadial (e.g. Salvigsen 1979; Salvigsen & Nydal 1981; Forman *et al.* 2004).

Cosmogenic exposure ages

Martensøya. – Sampling site 7ISL-2016-A2 is located on a ridge at the southernmost tip of a small mountain, Bratthovden (Fig. 1B). The bedrock ridge is situated between two raised beach plains to the northwest and east, respectively. A red, medium-grained erratic granite boulder was sampled at 85 m a.s.l. (Fig. 6A). The boulder yields an age of 14.7±1.82 ka (Fig. 7, Table 3). We interpret the age as the minimum age of the last deglaciation of this site.

Parryøya. – Three boulder samples and one bedrock sample were obtained from this site at 109–196 m a.s.l. The locality is the southern part of the mountain Øykollen (Figs 1B, 6B, E). Sample lithology is granite and migmatite. Samples 7ISL-2016-B28 (boulder) and 7ISL-2016-B29 (bedrock) are located ~50 m apart and yield ages of 44.36±3.63 and 43.49±4.59 ka, respectively (Fig. 7, Table 3). The ages overlap within the 1σ internal uncertainties, and we suggest the two samples experienced the same exposure history. Possibly the site was exposed in MIS 3, and not glacially eroded during MIS 2.

Samples 7ISL-2016-B31 (boulder; 196 m a.s.l.) and 7ISL-2016-B32 (boulder; 163 m a.s.l.) are located in the higher part of Parryøya ~500 m apart, and yield ages of 18.94±3.26 and 22.89±4.05 ka, respectively (Fig. 7, Table 3). The ages overlap within the 1σ internal

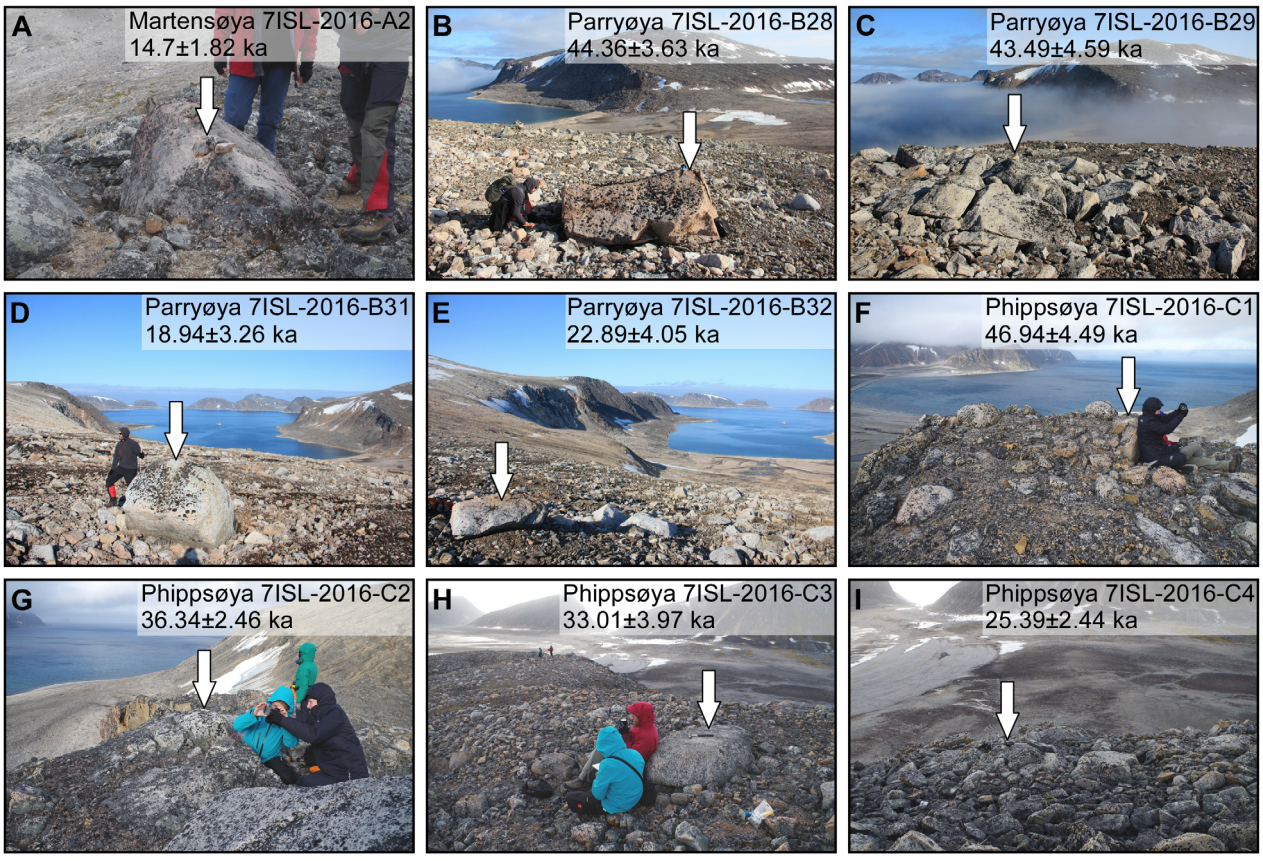

Fig. 6. Sampling localities for cosmogenic exposure dating. A. Martensøya, southwest Bratthovden (sample 7ISL-2016-A2). B–E. Parryøya, southeast Øykollen (samples 7ISL-2016-B28, 7ISL-2016-B29, 7ISL-2016-B31 and 7ISL-2016-B32). F–I. Phippsøya, southwest Høgberget (samples 7ISL-2016-C1, 7ISL-2016-C2, 7ISL-2016-C3 and 7ISL-2016-C4).

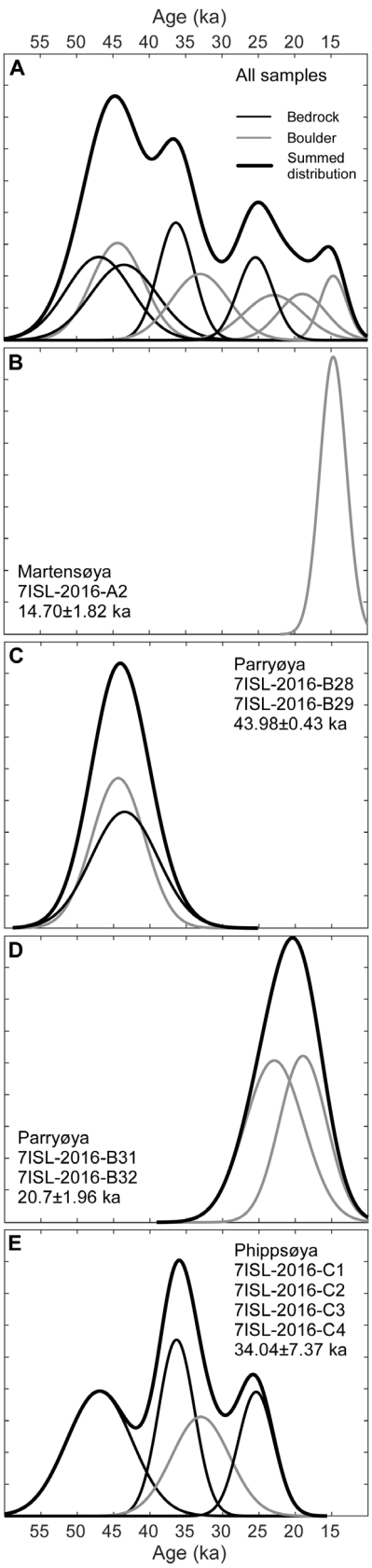

Fig. 7. Probability distributions of the ^{10}Be exposure ages of bedrock (black) and boulders (grey) from Sjuøyane. The ^{10}Be ages are presented as normal kernel density plots using the iceTEA tool (Jones *et al.* 2019). A. All ages. The summed distribution (bold) is shown even though a χ^2 test showed that there is less than 95% probability that the data set represents one population. When considering the ages as one population, the modal age is 44.72 ka and the weighted mean age is 29.5±11.25 ka. B. The sample from Martensøya (7ISL-2016-A2). C. The samples from Parryøya (7ISL-2016-B28 and 7ISL-2016-B29), sampled at the same locality. The weighted mean age is indicated. D. The samples from Parryøya (7ISL-2016-B31 and 7ISL-2016-B32). The weighted mean age is indicated. E. The samples from Phippsøya (7ISL-2016-C1, 7ISL-2016-C2, 7ISL-2016-C3 and 7ISL-2016-C4). The summed distribution (bold) is shown even though a χ^2 test showed that there is less than 95% probability that the data set represents one population.

uncertainties, and we suggest the two samples experienced the same exposure history. Assuming that the average age of 20.7±1.96 ka represents the time of the last deglaciation of the site, it suggests that at least the higher elevation parts of the area were ice-free at this time.

Phippsøya. – Three bedrock samples and one boulder sample were obtained from this site (Figs 1B, 6F, I). The locality is a hill on the southwestern part of the mountain Høgberget. Sample lithology is granite. The ages of the samples are 46.94±4.49 ka (bedrock; 7ISL-2016-C1), 36.34±2.46 ka (bedrock; 7ISL-2016-C2), 33.01±3.97 ka (boulder; 7ISL-2016-C3) and 25.39±2.44 ka (bedrock; 7ISL-2016-C4) (Fig. 7, Table 3). Two of the four ages overlap within the 1σ internal uncertainties, and we suggest the two samples experienced the same exposure history. However, the three oldest samples are of MIS 3 age, and indicate a complex exposure history. Possibly the site was exposed in MIS 3, and not glacially eroded during MIS 2.

Discussion

Sedimentary successions on Sjuøyane and implications for the glacial history

The majority of the sections consist of the (glacio-) marine and littoral sediments of LA 2 observed in all the sections on Phippsøya and Parryøya (Figs 4, 5), and the OSL ages indicate that LA2 was deposited during MIS 3 at Phippsøya (Fig. 8). The LA 2 sediments and the presence of the bedrock erosional notch with wave-washed bedrock and rounded boulders at 36±1 m a.h.t. on Phippsøya suggest that they formed during a high relative sea level, probably caused by glacio-isostatic depression following the MIS 4 glaciation of Svalbard (Forman & Ingólfsson 2000; Ingólfsson & Landvik 2013; Alexanderson *et al.* 2018). A MIS 3 age is supported by

Table 3. Summary of ^{10}Be data and cosmogenic exposure ages from Sjuøyane, Svalbard. See also Tables S5, S6 and Data S2.

Sample ID	Latitude (°N)	Longitude (°E)	Altitude (m a.s.l.)	Sample type	Lithology	Thickness (cm)	Shielding factor	Quartz (g)	^{9}Be carrier weight (g)	^{10}Be conc. (atoms g^{-1}) ×10^{4}	^{10}Be uncert. (atoms g^{-1}) ×10^{4}	^{10}Be age (ka)	1σ internal uncert. (ka)	1σ external uncert. (ka)
7ISL-2016-A2	80.68572	21.25531	85	Boulder	Granite	3.5	0.980146	20.2500	0.466153	6.214	0.775	14.70	1.82	1.9
7ISL-2016-B28	80.64578	20.62706	109	Boulder	Granite	4.5	1	24.1326	0.461330	19.357	1.593	44.36	3.63	3.99
7ISL-2016-B29	80.64632	20.62603	109	Bedrock	Granite	3	1	20.6757	0.463678	19.223	2.040	43.49	4.59	4.87
7ISL-2016-B31	80.64322	20.60873	196	Boulder	Granite	4	1	19.3073	0.465245	91.961	1.589	18.94	3.26	3.33
7ISL-2016-B32	80.64129	20.63376	163	Boulder	Migmatite	2.5	1	18.5122	0.465850	10.840	1.933	22.89	4.05	4.15
7ISL-2016-C1	80.70627	20.88935	81	Bedrock	Granite	1.5	0.999689	22.5029	0.459666	20.315	1.952	46.94	4.49	4.83
7ISL-2016-C2	80.70689	20.89089	105	Bedrock	Granite	4	0.998244	22.4189	0.463580	15.852	1.079	36.34	2.46	2.81
7ISL-2016-C3	80.70596	20.88905	113	Boulder	Granite	1	0.999168	20.6355	0.469480	14.921	1.803	33.01	3.97	4.16
7ISL-2016-C4	80.70505	20.88652	110	Bedrock	Granite	3.5	0.999168	20.1170	0.467665	11.226	1.086	25.39	2.44	2.62

our non-finite radiocarbon age Ua-54598 and radiocarbon age GX-22388 of Forman & Ingólfsson (2000) yielding a median age of 50.5 cal. ka BP from the same site in Horgvika (Tables 1, S1). Glaciomarine conditions during MIS 3 agree with the glacial history of western Spitsbergen and elsewhere on Svalbard, where e.g. marine sediments from the Kapp Ekholm interstadial demonstrate ice-free environments (Fig. 8C; Mangerud *et al.* 1998; Ingólfsson & Landvik 2013). Nordaustlandet was also ice-free during this Middle Weichselian interstadial, as indicated by the shallow marine or littoral sediments of Unit 6 in Isvika (Fig. 8D; Kaakinen *et al.* 2009), radiocarbon ages of marine bivalve shells from tills and marine sediments on NW Nordaustlandet (Blake 1989), and marine shell fragments emerging at the surface in Palanderbukta, SW Nordaustlandet (Schomacker *et al.* 2019).

Chauhan *et al.* (2016) analysed ice-rafted debris (IRD) in a marine sediment core from the shelf north-northeast of Nordaustlandet (HH11-09GC; Fig. 1). They suggested that the IRD peak during MIS 4 is caused by the advance of the SBIS (Fig. 8E), which agrees with the terrestrial evidence from Nordaustlandet (Kaakinen *et al.* 2009). The smaller IRD peak at the MIS 4/3 transition is interpreted to be caused by iceberg and/or sea-ice melting events during the disintegration of the SBIS. The IRD peak *c.* 30 cal. ka BP could reflect deposition from local slope failure rather than from icebergs, and it is not found in core JM10-02GC further southwest on the northern slope (Chauhan *et al.* 2016; Fig. 1). Our OSL ages suggest that the LA 2 sediments were still forming at this time (Fig. 8A). The IRD peaks during MIS 2 reflect the advancing SBIS at the LLGM and the deglaciation (Fig. 8E; Chauhan *et al.* 2016). The glacial drift above the postglacial marine limit described by Forman & Ingólfsson (2000) likely formed during the LLGM and its marine bivalve shell fragments dated to 42.7 cal. ka BP (Table S1) provides a maximum age. The source of the shells is likely to be the LA 2 sediments. We did not observe a glacial drift (basal till) in the sedimentological sections, and the stratigraphical association of the patchy glacial drift on the surface is not known. It might correlate to the diamict of LA 3. In Isvika, Nordaustlandet, a reddish basal till sandwiched between littoral sediments that were OSL dated to *c.* 40.0 and 10.6 ka, respectively, provides terrestrial evidence of a Late Weichselian glaciation in the region (Kaakinen *et al.* 2009). A detailed mapping of the distribution and sedimentology of the glacial drift on Sjuøyane could possibly provide data about the basal thermal conditions at the northern margin of the SBIS during deposition. Generally, the patchy glacial drift and well-preserved pre-Late Weichselian sediments suggest that the Late Weichselian glaciation was non-erosive and/or cold based, and probably of short duration. A similar pattern was observed on Nordaustlandet (Österholm 1990; Kaakinen *et al.* 2009). Together, these sites point towards

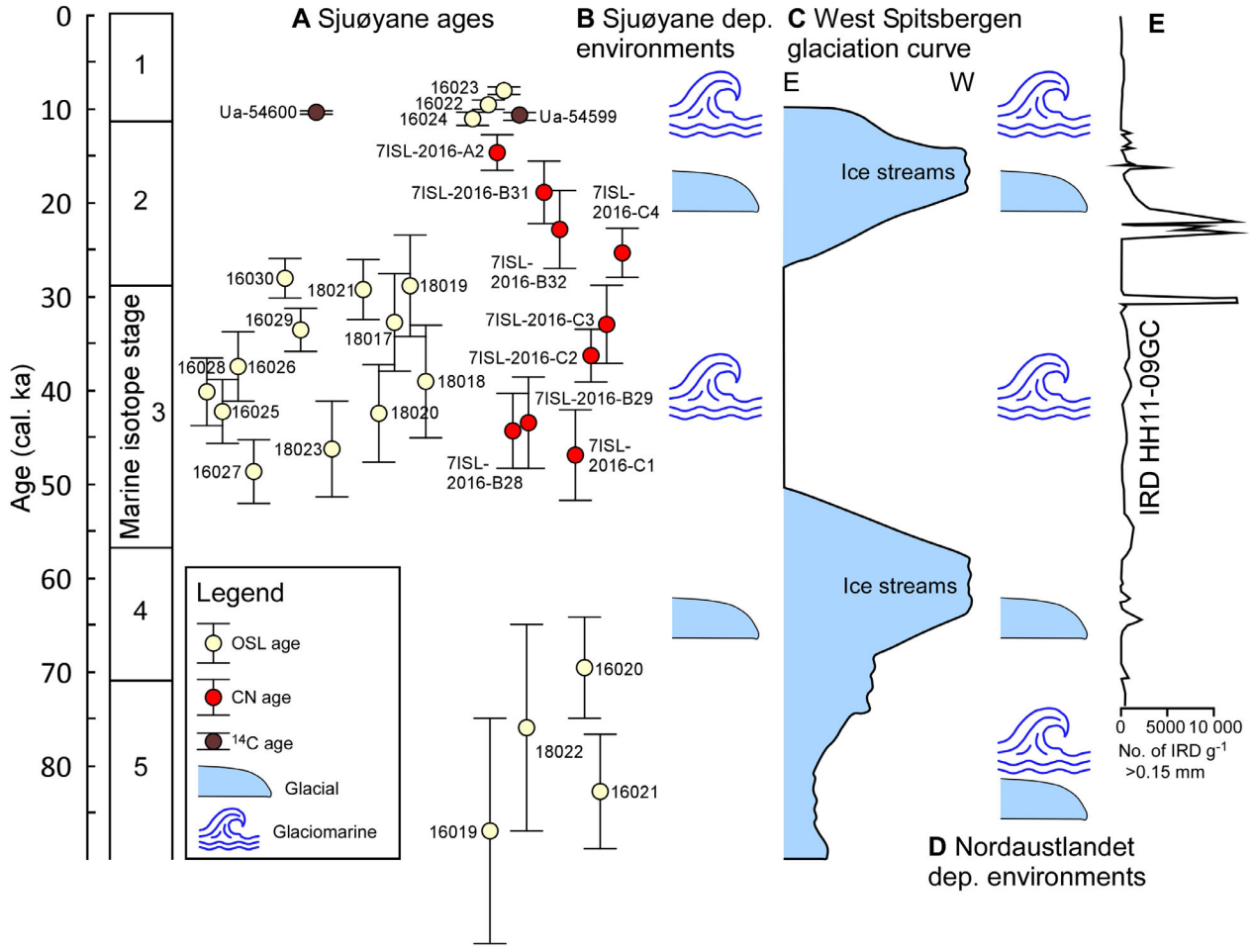

Fig. 8. A. Overview of the optically stimulated luminescence (OSL, in ka), radiocarbon (^{14}C, in cal. ka BP), and cosmogenic nuclide (CN, in ka) ages from Sjuøyane. B. Major depositional environments on Sjuøyane. C. Glaciation curve for western Spitsbergen after Mangerud *et al.* (1998) and Ingólfsson & Landvik (2013). D. Major depositional environments on Nordaustlandet (Isvika; Kaakinen *et al.* 2009). E. Concentration of ice-rafted debris (IRD) per gram dry weight of sediment in sediment core HH11-09GC at the northern Svalbard margin, northeast of Nordaustlandet (Chauhan *et al.* 2016).

limited Late Weichselian glacial activity along this part of the northern SBIS margin.

We interpret LA 4 on Phippsøya as prograding beach-face sediments deposited during regression (Fig. 4). At Trollodden, Forman & Ingólfsson (2000) radiocarbon dated a *Balanus balanus* sampled in a cliff section of sandy, littoral foreset beds grading into a raised beach, yielding a median age of 10.6 cal. ka BP (Table S1). This suggests that the LA 4 sediments were deposited during the last deglaciation. Similar sediments formed in Isvika, Nordaustlandet, at this time (Kaakinen *et al.* 2009) and at numerous other localities in Svalbard experiencing postglacial emergence (Forman *et al.* 2004). Althoughfiner-grained, the LA 2 sediments in Sandvika, Parryøya, corroborate the reconstruction of this environment (Fig. 5). These sediments formed during the Early Holocene in a sheltered bay during regression caused by the postglacial isostatic rebound. The LA 2 and 4 sediments and the postglacial marine limit at ~22±1 m a.h.t. provide clear terrestrial evidence of glaciation during the LLGM. Unfortunately, we were not able to find datable material on raised beaches to improve the postglacial relative sea level curve from Sjuøyane (Forman & Ingólfsson 2000). A better-constrained relative sea level curve from Sjuøyane could provide a better understanding of the glacio-isostatic rebound and, hence, the thickness and duration of glaciation at the north margin of the SBIS (e.g. Forman *et al.* 2004).

Cosmogenic exposure ages and implications for the glacial history

The nine exposure ages from Sjuøyane range from 46.94 to 14.70 ka (Figs 7, 8, Table 3), and the data set does not reveal a well-constrained deglaciation age for the archipelago. However, the ages provide information about the exposure history of each site. The two highest boulder samples (163 and 196 m a.s.l.) from Parryøya

overlap within 1σ and have an average age of 20.7±1.96 ka (Fig. 7D). They suggest that at least the higher parts of Sjuøyane were ice-free at this time. The boulder age of 14.70±1.82 ka from Martensøya (85 m a.s.l.) also indicates ice-free conditions by then (Fig. 7B). These data from Parryøya and Martensøya could support a conceptual glaciation model with active ice in the troughs on the continental shelf along the north margin of the SBIS and less active (or cold-based) ice between the troughs (Landvik *et al.* 2005; Ingólfsson & Landvik 2013). The remaining six exposure ages are LGM and older, and we do not interpret them as last deglaciation ages. At Parryøya, a bedrock (7ISL-2016-B29) and boulder (7ISL-2016-B28) age overlap within 1σ and have an average of 43.98 ka (Fig. 7C). Although samples 7ISL-2016-C2 and 7ISL-2016-C3 from Phippsøya overlap within 1σ, the scattered age distribution of the four samples from Phippsøya prevents a clear interpretation of the timing of the last deglaciation from the complex exposure history (Fig. 7E).

The low number of cosmogenic exposure ages from Sjuøyane restricts their significance for constraining the glacial history of Sjuøyane. We note that the youngest age of 14.70±1.82 ka from Martensøya is obtained from a red granite boulder (Fig. 6A) with a likely provenance from Nordaustlandet (Forman & Ingólfsson 2000). This would indicate active ice flow from the south during the Late Weichselian. It is likely that the samples that pre-date the last deglaciation are affected by inheritance and reflect repeated exposure during the Weichselian. A similar pattern of exposure ages was observed from highlands on Nordaustlandet, where boulders and bedrock samples consistently yielded ages older than the last deglaciation; however, without clustering significantly in other age intervals (Hormes *et al.* 2011). Hormes *et al.* (2011) interpreted the ages to be caused by cosmogenic isotope inheritance and suggested that the highlands experienced periods of non-erosive cold-based glaciation during the Weichselian. Hormes *et al.* (2011) suggested that the ^{10}Be exposure ages of 64–68 ka from highlands in Prins Oscars Land could reflect that the area was ice-free during MIS 2 and that the MIS 4 glaciation was more extensive. Similarly, ^{10}Be exposure ages from Amsterdamøya, NW Svalbard, suggest that the highlands (>300 m a.s.l.) were last glaciated >80 ka ago (Landvik *et al.* 2003). Our ^{10}Be ages from Sjuøyane are from MIS 2–3 (Fig. 8), and do not reveal whether this was also the case on Sjuøyane. However, the evidence of a higher relative sea level at 36±1 m a.h.t. on Phippsøya suggests that the archipelago was glacio-isostatically depressed at a time prior to the LGM. This could have been caused by glaciation during MIS 4.

Holocene environments

The lake sediments from Isvatnet show that organic sedimentation was taking place 7.0 cal. ka BP (Fig. 3, Table 1). Because datable material is lacking from the glaciolacustrine sediments (LU 1), we are not able to determine the age of this environment. However, Isvatnet is situated above the postglacial marine limit (Forman & Ingólfsson 2000), and it is likely that the glaciolacustrine sediments formed during the last deglaciation when meltwater last drained into the basin. The gyttja (LU 2) constituting the upper part of the lake sedimentary record shows constant sedimentation since 7.0 cal. ka BP (Fig. 3B) and no evidence of major environmental change.

On Parryøya, the two moss kill ages of 3.8 and 2.8 cal. ka BP (Fig. 2C, Table 1) suggest Neoglacial cooling, with expanding snow patches killing mosses growing near their margins. This agrees with ages of killed vegetation from central Spitsbergen, showing snowline lowering since at least 4.0–3.4 cal. ka BP (Miller *et al.* 2017) and with glacier expansion in northern Svalbard (Allaart *et al.* 2021).

Conclusions

- Terrestrial Quaternary geological data from Sjuøyane provide insight into the depositional environments during the Weichselian and Holocene. Our empirical data are important to validate and discuss conceptual and numerical models of the Svalbard–Barents Sea Ice Sheet, for example by providing ages and duration of ice-free periods (e.g. MIS 3) along the northern ice-sheet margin.
- Shallow marine and/or littoral sediments (LA 2) occur in the coastal sections of Phippsøya and Parryøya. Their ^{14}C and feldspar luminescence ages indicate ice-free conditions on Sjuøyane during MIS 3. The sediments formed during high relative sea level, most likely following the MIS 4 glaciation on Svalbard. On Parryøya, ^{14}C and OSL ages show that Sjuøyane were ice-free by *c.* 11.1 ka and that sedimentation took place in a shallow marine environment during regression caused by glacio-isostatic rebound. A bedrock erosional notch and rounded boulders provide evidence of a higher relative sea level at 36±1 m a.h.t. on Phippsøya. This level is higher than the postglacial marine limit and pre-dates the LGM.
- Red granite erratics on Sjuøyane indicate glacial transport from Nordaustlandet. One such granite boulder from lowlands on Martensøya yielded an age of 14.7±1.82 ka, reflecting the last deglaciation. Two boulder samples from Parryøya with ages of 18.94±3.26 and 22.89±4.05 ka suggest that the highlands were ice-free at this time. Cosmogenic nuclide datings of erratics and bedrock elsewhere on Sjuøyane pre-date the last deglaciation and reveal a complex exposure history, possibly due to repeated, cold-based glaciations. The patchy glacial drift at the

surface and the well-preserved pre-Late Weichselian sediments suggest non-erosive and/or cold-based Late Weichselian glaciation.

- *In situ*-killed moss sampled at the margin of a receding snow patch in Sandvika, Parryøya, yields radiocarbon median ages of 3.8 and 2.8 cal. ka BP. This indicates snow patch expansion in a deteriorating climate (Neoglacial cooling) at that time. Radiocarbon dating of a lacustrine sediment core from Isvatnet shows that gyttja has been accumulating at least since 7.0 cal. ka BP.
- The terrestrial northern margin of the Svalbard–Barents Sea Ice Sheet at Sjuøyane was characterized by non-erosive and/or cold-based glaciation during the LLGM. The pre-Late Weichselian relative sea level indicator at 36±1 m a.h.t. and ubiquitous raised marine sediments of MIS 3 age could indicate that the glaciation during MIS 4 was more extensive than during the Late Weichselian at this part of the Svalbard–Barents Sea Ice Sheet.

Acknowledgements. – Fieldwork at Sjuøyane was conducted during the University Centre in Svalbard (UNIS) graduate student course AG-348/848 in 2016 and 2018. For field assistance, we thank the students on the course, Anne E. Flink, and Marc Macias-Fauria. We thank Anna Hughes and an anonymous reviewer for constructive comments that improved the manuscript. The authors declare that they have no known competing financial interests or personal relationships that could have appeared to influence the work reported in this paper.

Author contributions. – AS: conceptualization, investigation, visualization, writing – original draft, project administration, funding acquisition. HA: conceptualization, investigation, visualization, writing – original draft, funding acquisition. WRF: investigation, writing – review & editing, funding acquisition. MFAF: investigation, writing – review & editing. SEK: investigation, visualization, writing – original draft. NK: investigation, writing – review & editing. ESE: investigation, writing – review & editing. RN: investigation, writing – review & editing. VJ: investigation, writing – review & editing. ÓI: writing – review & editing.

Data availability statement. – The data that support the findings of this study are available in the Supporting Information of this article.

References

Alexanderson, H. & Murray, A. S. 2012: Luminescence signals from modern sediments in a glaciated bay, NW Svalbard. *Quaternary Geochronology 10*, 250–256.

Alexanderson, H., Henriksen, M., Ryen, H. T., Landvik, J. Y. & Peterson, G. 2018: 200 ka of glacial events in NW Svalbard: an emergence cycle facies model and regional correlations. *Arktos 4*, 1–25.

Alexanderson, H., Landvik, J. Y. & Ryen, H. 2011: Chronology and styles of glaciation in an inter-fjord setting, northwestern Svalbard. *Boreas 40*, 175–197.

Allaart, L., Schomacker, A., Larsen, N. K., Nørmark, E., Rydningen, T. A., Farnsworth, W. R., Retelle, M., Brynjólfsson, S. & Kjellman, S. E. 2021: Glacial history of the Åsgardfonna Ice Cap, NE Spitsbergen, since the last glaciation. *Quaternary Science Reviews 251*, 106717, https://doi.org/10.1016/j.quascirev.2020.106717.

Balco, G., Stone, J. O., Lifton, N. A. & Dunai, T. J. 2008: A complete and easily accessible means of calculating surface exposure ages or erosion rates from ^{10}Be and ^{26}Al measurements. *Quaternary Geochronology 3*, 174–195.

Batchelor, C. L., Dowdeswell, J. A. & Hogan, K. A. 2011: Late quaternary ice flow and sediment delivery through Hinlopen Trough, Northern Svalbard margin: submarine landforms and depositional fan. *Marine Geology 284*, 13–27.

Benn, D. I. & Evans, D. J. A. 2010: *Glaciers and Glaciation*. 802 pp. Hodder Education, London.

Blaauw, M. & Christen, J. A. 2011: Flexible paleoclimate age-depth models using an autoregressive gamma process. *Bayesian Analysis 6*, 457–474.

Blake, W. J. 1961: Russian settlement and land rise in Nordaustlandet, Spitsbergen. *Arctic 14*, 101–111.

Blake, W. J. 1989: Radiocarbon dating by accelerator mass spectrometry; a contribution to the chronology of Holocene events in Nordaustlandet, Svalbard. *Geografiska Annaler 71 A*, 59–74.

Bluck, B. J. 1999: Clast assembling, bed-forms and structure in gravel beaches. *Transactions of the Royal Society of Edinburgh, Earth Science 89*, 291–323.

Bondevik, S. 1993: *Postglasial strandforskyvning på Svalbard*. Unpublished Cand. Scient. thesis, University of Bergen, 81 pp.

Braucher, R., Guillou, V., Bourlès, D. L., Arnold, M., Aumaître, G., Keddadouche, K. & Nottoli, E. 2015: Preparation of ASTER in-house ^{10}Be/^{9}Be standard solutions. *Nuclear Instruments and Methods in Physics Research B 361*, 335–340.

Briner, J. P., Miller, G. H., Davis, P. T. & Finkel, R. C. 2006: Cosmogenic radionuclides from fiord landscapes support differential erosion by overriding ice sheets. *GSA Bulletin 118*, 406–420.

Buylaert, J. P., Murray, A. S., Thomsen, K. J. & Jain, M. 2009: Testing the potential of an elevated temperature IRSL signal from K-feldspar. *Radiation Measurements 44*, 560–565.

Chauhan, T., Rasmussen, T. L. & Noormets, R. 2016: Palaeoceanography of the Barents Sea continental margin, north of Nordaustlandet, Svalbard, during the last 74 ka. *Boreas 45*, 76–99.

Chauhan, T., Rasmussen, T. L., Noormets, R., Jakobsson, M. & Hogan, K. A. 2014: Glacial history and paleoceanography of the southern Yermak Plateau since 132 ka BP. *Quaternary Science Reviews 92*, 155–169.

Chmeleff, J., von Blanckenburg, F., Kossert, K. & Jakob, D. 2010: Determination of the ^{10}Be half-life by multicollector ICP-MS and liquid scintillation counting. *Nuclear Instruments and Methods in Physics Research Section B: Beam Interactions with Materials and Atoms 268*, 192–199.

Corbett, L., Bierman, P., Graly, J., Neumann, T. & Rood, D. 2013: Constraining landscape history and glacial erosivity using paired cosmogenic nuclides in Upernavik, northwest Greenland. *GSA Bulletin 125*, 1539–1553.

Dallmann, W. K. (ed.) 2015: Geoscience Atlas of Svalbard. *Norwegian Polar Institute Report Series 148*, 1–292.

Donner, J. J. & West, R. G. 1957: The Quaternary geology of Brageneset, Nordaustlandet, Spitsbergen. *Norsk Polarinstitutt Skrifter 109*, 1–29.

Dowdeswell, J. A., Hogan, K. A., Evans, J., Noormets, R., Ó Cofaigh, C. & Ottesen, D. 2010: Past ice-sheet flow east of Svalbard inferred from streamlined subglacial landforms. *Geology 38*, 163–166.

Durcan, J. A., King, G. E. & Duller, G. A. T. 2015: DRAC: dose rate and age calculator for trapped charge dating. *Quaternary Geochronology 28*, 54–61.

Evans, D. J. A. & Benn, D. I. 2004: *A Practical Guide to the Study of Glacial Sediments*. 266 pp. Arnold, London.

Eyles, N., Eyles, C. H. & Miall, A. D. 1983: Lithofacies types and vertical profile models; an alternative approach to the description and environmental interpretation of glacial diamict and diamictite sequences. *Sedimentology 30*, 393–410.

Forman, S. L. & Ingólfsson, Ó. 2000: Late Weichselian glacial history and postglacial emergence of Phippsøya, Sjuøyane, northern Svalbard: a comparison of modelled and empirical estimates of a glacial-rebound hinge line. *Boreas 29*, 16–25.

Forman, S. L., Lubinski, D. J., Ingólfsson, Ó., Zeeberg, J. J., Snyder, J. A., Siegert, M. J. & Matishov, G. G. 2004: A review of postglacial emergence on Svalbard, Franz Josef Land and Novaya Zemlya, northern Eurasia. *Quaternary Science Reviews 23*, 1391–1434.

Fransner, O., Noormets, R., Chauhan, T., O'Regan, M. & Jakobsson, M. 2018: Late Weichselian ice stream configuration and dynamics in Albertini Trough, northern Svalbard margin. *Arktos 4*, 1–22.

Fransner, O., Noormets, R., Flink, A. E., Hogan, K. A., O'Regan, M. & Jakobsson, M. 2017: Glacial landforms and their implications for glacier dynamics in Rijpfjorden and Duvefjorden, northern Nordaustlandet, Svalbard. *Journal of Quaternary Science 32*, 437–455.

Gjermundsen, E. F., Briner, J. P., Akcar, N., Foros, J., Kubik, P. W., Salvigsen, O. & Hormes, A. 2015: Minimal erosion of Arctic alpine topography during late Quaternary glaciation. *Nature Geoscience 8*, 789–793.

Gosse, J. C. & Phillips, F. M. 2001: Terrestrial in situ cosmogenic nuclides: theory and application. *Quaternary Science Reviews 20*, 1475–1560.

Heaton, T. J., Köhler, P., Butzin, M., Bard, E., Reimer, R. W., Austin, W. E. N., Bronk Ramsey, C., Grootes, P. M., Hughen, K. A., Kromer, B., Reimer, P. J., Adkins, J., Burke, A., Cook, M. S., Olsen, J. & Skinner, L. C. 2020: Marine20 – the marine radiocarbon age calibration curve (0–55,000 cal BP). *Radiocarbon 62*, 779–820.

Hogan, K. A., Dowdeswell, J. A., Hillenbrand, C.-D., Ehrmann, W., Noormets, R. & Wacker, L. 2017: Subglacial sediment pathways and deglacial chronology of the northern Barents Sea Ice Sheet. *Boreas 46*, 750–771.

Hogan, K. A., Dowdeswell, J. A., Noormets, R., Evans, J., Ó Cofaigh, C. & Jakobsson, M. 2010: Submarine landforms and ice-sheet flow in the Kvitøya Trough, northwestern Barents Sea. *Quaternary Science Reviews 29*, 3545–3562.

Hormes, A., Akcar, N. & Kubik, P. W. 2011: Cosmogenic radionuclide dating indicates ice-sheet configuration during MIS 2 on Nordaustlandet, Svalbard. *Boreas 40*, 636–649.

Huntley, D. & Baril, M. 1997: The K content of the K-feldspars being measured in optical dating or in thermoluminescence dating. *Ancient TL 15*, 11–13.

Huntley, D. J. & Lamothe, M. 2001: Ubiquity of anomalous fading in K-feldspars and the measurement and correction for it in optical dating. *Canadian Journal of Earth Sciences 38*, 1093–1106.

Ingólfsson, Ó. 2011: Fingerprints of Quaternary glaciations on Svalbard. *In* Martini, I. P., French, H. M. & Pérez Alberti, A. (eds.): *Ice-Marginal and Periglacial Processes and Sediments*, 15–31. *Geological Society, London, Special Publications 354*.

Ingólfsson, Ó. & Landvik, J. Y. 2013: The Svalbard-Barents Sea ice-sheet – historical, current and future perspectives. *Quaternary Science Reviews 64*, 33–60.

Jakobsson, M. and 51 others 2020: The International Bathymetric Chart of the Arctic Ocean version 4.0. *Scientific Data 7*, 176, https://doi.org/10.1038/s41597-020-0520-9.

Jones, R. S., Small, D., Cahill, N., Bentley, M. J. & Whitehouse, P. L. 2019: iceTEA: tools for plotting and analysing cosmogenic-nuclide surface-exposure data from former ice margins. *Quaternary Geochronology 51*, 72–86.

Kaakinen, A., Salonen, V.-P., Kubischta, F., Eskola, K. O. & Oinonen, M. 2009: Weichselian glacial stage in Murchinsonfjorden, Nordaustlandet, Svalbard. *Boreas 38*, 718–729.

Kars, R. H., Reimann, T., Ankjærgaard, C. & Wallinga, J. 2014: Bleaching of the post-IR IRSL signal: new insights for feldspar luminescence dating. *Boreas 43*, 780–791.

Kirchner, N., Noormets, R., Kuttenkeuler, J., Erstorp, E. S., Holmlund, E. S., Rosqvist, G., Holmlund, P., Wennbom, M. & Karlin, T. 2019: High-resolution bathymetric mapping reveals subaqueous glacial landforms in the Arctic alpine lake Tarfala, Sweden. *Journal of Quaternary Science 34*, 452–462.

Kleiber, H. P., Knies, J. & Niessen, F. 2000: The Late Weichselian glaciation of the Franz Victoria Trough, northern Barents Sea: ice sheet extent and timing. *Marine Geology 168*, 25–44.

Knies, J., Kleiber, H.-P., Matthiessen, J., Müller, C. & Nowaczyk, N. 2001: Marine ice-rafted debris records constrain maximum extent of Saalian and Weichselian ice-sheets along the northern Eurasian margin. *Global and Planetary Change 31*, 45–64.

Korschinek, G., Bergmaier, A., Faestermann, T., Gerstmann, U. C., Knie, K., Rugel, G., Wallner, A., Dillmann, I., Dollinger, G., von Gostomski, C. L., Kossert, K., Maiti, M., Poutivtsev, M. & Remmert, A. 2010: A new value for the half-life of ^{10}Be by heavy-ion elastic recoil detection and liquid scintillation counting. *Nuclear Instruments and Methods in Physics Research Section B: Beam Interactions with Materials and Atoms 268*, 187–191.

Kreutzer, S. 2018: calc_FadingCorr(): apply a fading correction according to Huntley & Lamothe (2001) for a given g-value and a given tc. *In* Kreutzer, S., Burow, C., Dietze, M., Fuchs, M. C., Schmidt, C., Fischer, M. & Friedrich, J. (eds.): *Luminescence: Comprehensive Luminescence Dating Data Analysis. R package version 0.8.6*. Available at: https://cran.r-project.org/web/packages/Luminescence/index.html

Krüger, J. & Kjær, K. H. 1999: A data chart for field description and genetic interpretation of glacial diamicts and associated sediments – with examples from Greenland, Iceland, and Denmark. *Boreas 28*, 386–402.

Lal, D. 1991: Cosmic ray labeling of erosion surfaces: in situ nuclide production rates and erosion models. *Earth and Planetary Science Letters 104*, 424–439.

Landvik, J. Y., Bondevik, S., Elverhøi, A., Fjeldskaar, W., Mangerud, J., Siegert, M. J., Salvigsen, O., Svendsen, J.-I. & Vorren, T. O. 1998: The last glacial maximum of Svalbard and the Barents Sea area: ice sheet extent and configuration. *Quaternary Science Reviews 17*, 43–75.

Landvik, J. Y., Brook, E. J., Gualtieri, L., Raisbeck, G., Salvigsen, O. & Yiou, F. 2003: Northwest Svalbard during the last glaciation: ice-free areas existed. *Geology 31*, 905–908.

Landvik, J. Y., Ingólfsson, Ó., Mienert, J., Lehman, S. J., Solheim, A., Elverhøi, A. & Ottesen, D. 2005: Rethinking Late Weichselian ice-sheet dynamics in coastal NW Svalbard. *Boreas 34*, 7–24.

Leirdal, G. 1997: *Senkvartær utvikling av kontinentalmarginen nord for Svalbard*. Cand. Scient. thesis, University of Oslo, 141 pp.

Mangerud, J., Dokken, T., Hebbeln, D., Heggen, B., Ingólfsson, Ó., Landvik, J. Y., Mejdahl, V., Svendsen, J. I. & Vorren, T. O. 1998: Fluctuations of the Svalbard-Barents Sea Ice Sheet during the last 150 000 years. *Quaternary Science Reviews 17*, 11–42.

Martin, L. C. P., Blard, P.-H., Balco, G., Lavé, J., Delunel, R., Lifton, N. & Laurent, V. 2017: The CREp program and the ICE-D production rate calibration database: a fully parameterizable and updated online tool to compute cosmic-ray exposure ages. *Quaternary Geochronology 38*, 25–49.

Merchel, S. & Herpers, U. 1999: An update on radiochemical separation techniques for the determination of long-lived radionuclides via accelerator mass spectrometry. *Radiochimica Acta 84*, 215–219.

Miller, G. H., Landvik, J. Y., Lehman, S. J. & Southon, J. R. 2017: Episodic Neoglacial snowline descent and glacier expansion on Svalbard reconstructed from the ^{14}C ages of ice-entombed plants. *Quaternary Science Reviews 155*, 67–78.

Nishiizumi, K., Imamura, M., Caffee, M. W., Southon, J. R., Finkel, R. C. & McAninch, J. 2007: Absolute calibration of ^{10}Be AMS standards. *Nuclear Instruments and Methods in Physics Research Section B: Beam Interactions with Materials and Atoms 258*, 403–413.

Norwegian Polar Institute 2014: *Terrengmodell Svalbard (S0 Terrengmodell) (Data set)*. Norwegian Polar Institute, Tromsø, https://doi.org/10.21334/npolar.2014.dce53a47.

Norwegian Polar Institute 2017: *S100 Topographic Raster Data for Svalbard (Data set)*. Norwegian Polar Institute, Tromsø, https://doi.org/10.21334/npolar.1990.44ca8c2a.

Ó Cofaigh, C. & Dowdeswell, J. A. 2001: Laminated sediments in glacimarine environments: diagnostic criteria for their interpretation. *Quaternary Science Reviews 20*, 1411–1436.

Österholm, H. 1990: The Late Weichselian glaciation and Holocene shore displacement on Prins Oscars Land, Nordaustlandet, Svalbard. *Geografiska Annaler 72A*, 301–317.

Ottesen, D., Dowdeswell, J. A., Landvik, J. Y. & Mienert, J. 2007: Dynamics of the Late Weichselian ice sheet on Svalbard inferred from high-resolution sea-floor morphology. *Boreas 36*, 286–306.

Patton, H., Andreassen, K., Bjarnadóttir, L. R., Dowdeswell, J. A., Winsborrow, M. C. M., Noormets, R., Polyak, L., Auriac, A. & Hubbard, A. 2015: Geophysical constraints on the dynamics and retreat of the Barents Sea ice sheet as a paleobenchmark for models of marine ice sheet deglaciation. *Reviews of Geophysics 53*, 1051–1098.

Patton, H., Hubbard, A., Andreassen, K., Winsborrow, M. & Stroeven, A. P. 2016: The build-up, configuration, and dynamical sensitivity of the Eurasian ice-sheet complex to Late Weichselian climatic and oceanic forcing. *Quaternary Science Reviews 153*, 97–121.

Pieńkowski, A. J., Husum, K., Furze, M. F., Missana, A. F., Irvalı, N., Divine, D. V. & Eilertsen, V. T. 2022: Revised ΔR values for the Barents Sea and its archipelagos as a pre-requisite for accurate and robust marine-based ^{14}C chronologies. *Quaternary Geochronology 68*, 101244, https://doi.org/10.1016/j.quageo.2021.101244.

R Core Team 2021: *R: A Language and Environment for Statistical Computing*. R Foundation for Statistical Computing, Vienna. 2016. Available at: https://www.Rproject.org/.

Reimer, P. J. and 38 others 2020: The IntCal20 northern hemisphere radiocarbon age calibration curve (0-55 cal kBP). *Radiocarbon 62*, 725–757.

Salvigsen, O. 1979: The last deglaciation of Svalbard. *Boreas 8*, 229–231.

Salvigsen, O. & Nydal, R. 1981: The Weichselian glaciation in Svalbard before 15,000 BP. *Boreas 10*, 433–446.

Schomacker, A., Farnsworth, W. R., Ingólfsson, Ó., Allaart, L., Håkansson, L., Retelle, M., Siggaard-Andersen, M.-L., Korsgaard, N. J., Rouillard, A. & Kjellman, S. E. 2019: Postglacial relative sea level change and glacier activity in the early and late Holocene: Wahlenbergfjorden, Nordaustlandet, Svalbard. *Scientific Reports 9*, 6799, https://doi.org/10.1038/s41598-019-43342-z.

Stone, J. O. 2000: Air pressure and cosmogenic isotope production. *Journal of Geophysical Research 105*, 23753–23759.

Strzelecki, M. C., Long, A. J., Lloyd, J. M., Malecki, J., Zagorski, P., Pawlowski, L. & Jaskolski, M. W. 2018: The role of rapid glacier retreat and landscape transformation in controlling the post-Little Ice Age evolution of paraglacial coasts in central Spitsbergen (Billefjorden, Svalbard). *Land Degradation and Development 29*, 1962–1978.

Svendsen, J. I., Alexanderson, H., Astakhov, V. I., Demidov, I., Dowdeswell, J. A., Funder, S., Gataullin, V., Henriksen, M., Hjort, C., Houmark-Nielsen, M., Hubberten, H. W., Ingólfsson, Ó., Jakobsson, M., Kjær, K. H., Larsen, E., Lokrantz, H., Lunkka, J. P., Lysså, A., Mangerud, J., Matiouchkov, A., Murray, A., Möller, P., Niessen, F., Nikolskaya, O., Polyak, L., Saarnisto, M., Siegert, C., Siegert, M. J., Spielhagen, R. F. & Stein, R. 2004: Late Quaternary ice sheet history of northern Eurasia. *Quaternary Science Reviews 23*, 1229–1271.

Vacek, F., Deutsch, C., Kuttenkeuler, J. & Kirchner, N. In press: Short-term calving front dynamics and mass loss at Sálajiegna glacier, northern Sweden, assessed by uncrewed surface and aerial vehicles. *Journal of Glaciology*, https://doi.org/10.1017/jog.2024.34.

Young, N. E., Schaefer, J. M., Briner, J. & Goehring, B. M. 2013: ^{10}Be production-rate calibration for the Arctic. *Journal of Quaternary Science 28*, 516–526.

Supporting Information

Additional Supporting Information to this article is available at http://www.boreas.dk.

Data S1. Preparation, measurement, and age calculation for luminescence samples.

Data S2. Raw data for calculation of ^{10}Be exposure ages.

Fig. S1. Examples of growth and decay curves from sample 16029 (1-mm aliquots).

Fig. S2. Dose recovery for A. IR_{50} and B. $pIRIR_{225}$. Ideally the measured dose should equal the given dose within ±10%.

Fig. S3. Examples of fading determinations, here sample 16029.

Fig. S4. Abanico plots of the dose distributions for sample 16029 (1-mm aliquots).

Table S1. Re-calibrated radiocarbon ages from Sjuøyane, Nordaustlandet, and the continental shelf and upper slope north of Nordaustlandet, Svalbard. Ages from publications are re-calibrated in OxCal v4.4. using Marine20 (Heaton *et al*. 2020) and a ΔR value of −61±37 years for shells and foraminifera and −160±41 years for whalebones (Pieńkowski *et al*. 2022). All radiocarbon ages are shown in the table with reference to the original study.

Table S2. Dose rate data. Sediment nuclide concentrations as determined from high-resolution gamma spectrometry, cosmic dose rate and total environmental dose rate calculated in DRAC (Durcan *et al*. 2015), and sediment water content (field, saturated, and estimated average since time of deposition).

Table S3. $pIRIR_{225}$ luminescence data. Corrected ages are corrected for fading according to Huntley & Lamothe (2001) using the calc_FadingCorr() function in the RLuminescence package (Kreutzer 2021). The residual dose has not been subtracted.

Table S4. IR_{50} luminescence data. Corrected ages are corrected for fading according to Huntley & Lamothe (2001) using the calc_FadingCorr function in the RLuminescence package (Kreutzer 2021). The residual dose has not been subtracted.

Table S5. Full ^{10}Be data set and data for calculation of cosmogenic exposure ages from Sjuøyane, Svalbard.

Table S6. Full ^{10}Be data set and data for calculation of cosmogenic exposure ages from Sjuøyane, Svalbard.